# Cooperativity in the Iron(II) Spin-Crossover Compound $[Fe(ptz)_6](PF_6)_2$ under the Influence of External Pressure (ptz = 1-*n*-Propyltetrazole)

**Jelena Jeftić,[†] Roland Hinek,[‡] Silvia C. Capelli,[§] and Andreas Hauser*,[||]**

Departement für Chemie und Biochemie, Universität Bern, Freiestrasse 3, CH-3000 Bern 9, Switzerland, Institut für Anorganische Chemie und Analytische Chemie, Johannes Gutenberg-Universität, Staudinger Weg 9, D-55099 Mainz, Germany, Laboratorium für chemische und mineralogische Kristallographie, Universität Bern, Freiestrasse 3, CH-3000 Bern 9, Switzerland, and Département de chimie physique, Université de Genève, 30, Quai Ernest-Ansermet, CH-1211 Genève 4, Switzerland

*Received November 22, 1996*[⊗]

The iron(II) spin-crossover compound $[Fe(ptz)_6](PF_6)_2$ (ptz = 1-propyltetrazole) crystallizes in the triclinic space group $P\bar{1}$, with $a = 10.6439(4)$ Å, $b = 10.8685(4)$ Å, $c = 11.7014(4)$ Å, $\alpha = 75.644(1)°$, $\beta = 71.671(1)°$, $\gamma = 60.815(1)°$, and $Z = 1$. In $[Fe(ptz)_6](PF_6)_2$, the thermal spin transition is extremely steep because of cooperative effects of elastic origin. The transition temperature at ambient pressure is 74(1) K. An external pressure of 1 kbar shifts the transition temperature to 102(1) K, corresponding to a stabilization of the low-spin state, which is smaller in volume. The volume difference between the high-spin and the low-spin state, $\Delta V^{\circ}_{HL}$, is 24(2) Å$^3$/molecule. The interaction constant $\Gamma$, as a measure of cooperativity, is within experimental error independent of external pressure and has a value of 101(5) cm$^{-1}$. In contrast to the case of the related compound $[Fe(ptz)_6](BF_4)_2$ (Decurtins et al. *Inorg. Chem.* **1985**, *24*, 2174), there is no hysteresis due to a first-order crystallographic phase transition, nor is there a hysteresis induced by external pressure as in the mixed crystal $[Zn_{1-x}Fe_x(ptz)_6](BF_4)_2$, $x = 0.1$ (Jeftić et al. *J. Phys. Chem. Solids* **1996**, *57*, 1743). However, in $[Fe(ptz)_6](PF_6)_2$, the interaction constant $\Gamma$ is found to be very close to the critical value above which a hysteresis solely due to the cooperative effects is expected. In addition, high-spin → low-spin relaxation measurements were performed under external pressures of up to 1 kbar in the temperature interval between 50 and 60 K. An external pressure of 1 kbar accelerates the high-spin → low-spin relaxation by 1 order of magnitude.

## Introduction

Iron(II) complexes which show a thermal spin transition from the $^1A_1$ low-spin (LS) state at low temperatures to the $^5T_2$ high-spin (HS) state at elevated temperatures, so-called spin-crossover complexes,[1,2] are well suited for pressure studies.[3−19] The difference in volume, $\Delta V^{\circ}_{HL} = V_{HS} - V_{LS}$, between HS and LS complexes is comparatively large[20−22] due to the large difference in metal−ligand bond lengths, $\Delta r^{\circ}_{HL} = r_{HS} - r_{LS} \approx 0.16-0.21$ Å.[23−26] Therefore, the contribution of the work term, $p\Delta V^{\circ}_{HL}$, to the Gibbs free energy is already significant for small external pressures of up to 1 kbar.[27,28] In addition to influencing the spin equilibrium, such external pressures affect the kinetics of the HS → LS relaxation.[19,29−32]

The neat spin-crossover compound $[Fe(ptz)_6](BF_4)_2$ and its corresponding mixed-crystal series $[Zn_{1-x}Fe_x(ptz)_6](BF_4)_2$, which are closely related to the title compound, have been the subject

[†] Departement für Chemie und Biochemie, Universität Bern.
[‡] Johannes Gutenberg-Universität.
[§] Laboratorium für chemische und mineralogische Kristallographie, Universität Bern.
[||] Université de Genève.
[⊗] Abstract published in *Advance ACS Abstracts*, June 1, 1997.

(1) Gütlich, P. *Struct. Bonding* **1981**, *44*, 83.
(2) Gütlich, P.; Hauser, A.; Spiering, H. *Angew. Chem., Int. Ed. Engl.* **1994**, *33*, 2024.
(3) Slichter, C. P.; Drickamer, H. G. *J. Chem. Phys.* **1972**, *56*, 2142.
(4) Fisher, D. C.; Drickamer, H. G. *J. Chem. Phys.* **1971**, *54*, 4825.
(5) Adams, D. M.; Long, G. J.; Williams, A. D. *Inorg. Chem.* **1982**, *21*, 1049.
(6) Meissner, E.; Köppen, H.; Spiering, H.; Gütlich, P. *Chem. Phys. Lett.* **1983**, *95*, 163.
(7) Pebler, J. *Inorg. Chem.* **1983**, *22*, 4125.
(8) König, E.; Ritter, G.; Kulshreshtha, S. K.; Waigel, J.; Goodwin, H. A. *Inorg. Chem.* **1984**, *23*, 1896.
(9) König, E.; Ritter, G.; Waigel, J.; Goodwin, H. A. *J. Chem. Phys.* **1985**, *83*, 3055.
(10) Usha, S.; Srinivasan, R.; Rao, C. N. *Chem. Phys.* **1985**, *100*, 447.
(11) (a) Meissner, E.; Köppen, H.; Köhler, C. P.; Spiering, H.; Gütlich P. *Hyperfine Interact.* **1986**, *28*, 799. (b) *Ibid.* **1987**, *36*, 1.
(12) Long, G. J.; Hutchinson, B. B. *Inorg. Chem.* **1987**, *26*, 608.
(13) Köppen, H.; Meissner, E.; Wiehl, L.; Spiering, H.; Gütlich, P. *Hyperfine Interact.* **1989**, *52*, 29.
(14) McCusker, J. K.; Zvagulis, M.; Drickamer, H. G.; Hendrickson, D. N. *Inorg. Chem.* **1989**, *28*, 1380.
(15) Konno, M.; Mikami-Kido, M. *Bull. Chem. Soc. Jpn.* **1991**, *64*, 339.
(16) Granier, T.; Gallois, B.; Gauthier, J.; Real, J.-A.; Zarembowitch, J. *Inorg. Chem.* **1993**, *32*, 5305.
(17) König, E.; Ritter, G.; Grünstreudel, H.; Dengler, J.; Nelson, J. *Inorg. Chem.* **1994**, *33*, 837.
(18) McGarvey, J. J.; Lawthers, I.; Heremans, K.; Toftlund, H. *J. Chem. Soc., Chem. Commun.* **1984**, 1575.
(19) Roux, C.; Zarembowitch, J.; Itie, J.-P.; Polian, A.; Verdaguer, M. *Inorg. Chem.* **1996**, *35*, 574.
(20) Wiehl, L.; Spiering, H.; Gütlich, P.; Knorr, K. *J. Appl. Crystallogr.* **1984**, *23*, 151.
(21) Wiehl, L.; Kiel, G.; Köhler, C. P.; Spiering, H.; Gütlich, P. *Inorg. Chem.* **1986**, *25*, 1565.
(22) Binstead, R. A.; Beattie, J. K. *Inorg. Chem.* **1986**, *25*, 1481.
(23) Hoselton, M. A.; Wilson, L. J.; Drago, R. S. *J. Am. Chem. Soc.* **1975**, *97*, 1722.
(24) Mikami-Kido, M.; Saito, Y. *Acta Crystallogr.* **1982**, *B38*, 452.
(25) Katz, B. A.; Strouse, C. E. *J. Am. Chem. Soc.* **1979**, *101*, 6214.
(26) Gallois, B.; Real, J. A.; Hauw, C.; Zarembowitch, J. *Inorg. Chem.* **1990**, *29*, 1152.
(27) Jeftić, J.; Hauser, A. *Chem. Phys. Lett.* **1996**, *248*, 458.
(28) Jeftić, J.; Romstedt, H.; Hauser, A. *J. Phys. Chem. Solids* **1996**, *57*, 1743.
(29) DiBenedetto, J.; Arkle, V.; Goodwin, H. A.; Ford, P. C. *Inorg. Chem.* **1985**, *24*, 456.
(30) Adler, P.; Hauser, A.; Vef, A.; Spiering, H.; Gütlich, P. *Hyperfine Interact.* **1989**, *47*, 343.
(31) Adler, P.; Spiering, H.; Gütlich, P. *J. Phys. Chem. Solids* **1989**, *50*, 587.
(32) McGarvey, J. J.; Lawthers I.; Heremans, K.; Toftlund H. *Inorg. Chem.* **1990**, *29*, 252.

S0020-1669(96)01404-8 CCC: $14.00 

of a number of studies on the thermal spin transition[27,28,33−35] as well as on the photophysical properties[36,37] and the dynamics of the HS → LS relaxation.[27,38,39] In addition to these, a structural study[40] revealed that the hysteresis in the thermal spin transition ($T_c\downarrow = 128$ K, $T_c\uparrow = 135$ K) is due to a first-order crystallographic phase transition from $R\bar{3}$ above $T_c\uparrow$ to $P\bar{1}$ below $T_c\downarrow$. Whereas Jung et al.[34,35] give a detailed account of the cooperative effects of elastic origin[41] on the thermal spin transition of $[Zn_{1-x}Fe_x(ptz)_6](BF_4)_2$, $0.01 \leq x \leq 1$, in the supercooled high-symmetry phase, Jeftić et al.[28] discuss the interplay between the spin transition and the crystallographic phase transition. In the diluted system, the crystallographic phase transition can be induced by an external pressure.[28]

Cooperative effects give rise to a strongly self-accelerating HS → LS relaxation behavior in the neat material.[38,39] The cooperative effects may be pictured as a buildup of an internal pressure during the relaxation process. In much the same way an external pressure was found to accelerate the HS → LS relaxation in the diluted compound $[Zn_{1-x}Fe_x(ptz)_6](BF_4)_2$, $x = 0.1$, by 1 order of magnitude at 1 kbar and $T = 40$ K.[27]

Because of the complexity of the $[Zn_{1-x}Fe_x(ptz)_6](BF_4)_2$ system (interplay between crystallographic phase transition and spin transition, pressure-induced phase transition), a comprehensive treatment of the spin equilibrium in all phases together with the dynamics of the HS → LS relaxation is a taunting task. The title compound, $[Fe(ptz)_6](PF_6)_2$, does not show a first-order crystallographic phase transition (vide infra). It is thus more amenable to such a treatment. In this paper, we present the crystal structure of the title compound at 130 K and its photophysical properties. Thermal spin transition curves between ambient pressure and 1 kbar and HS → LS relaxation curves in the same pressure range are discussed comprehensively.

## Experimental Section

**1. Preparation of $[Fe(ptz)_6](PF_6)_2$ and Crystal Growth.** $[Fe(ptz)_6](PF_6)_2$ was prepared by the procedure previously described, but with $HPF_6$ instead of $HBF_4$.[33] Well-shaped single crystals were grown from saturated solutions in nitromethane by slow evaporation of the solvent. The crystals are slightly bluish due to the broad absorption band of the $^5T_2 \rightarrow {}^5E$ transition in the near-infrared, with its tail extending into the visible region, and are formed as hexagonal plates up to several millimeters in diameter and about 0.5 mm thick.

**2. Structure Determination.** For the X-ray structure determination, a piece of dimensions $0.5 \times 0.3 \times 0.1$ mm$^3$ was chipped off one of the larger crystals with a razor blade. The crystals have a cleavage plane perpendicular to the pseudo-hexagonal axis. This makes it very difficult to cut a crystal perpendicular to it without introducing a substantial mosaic structure.

The relevant structure determination parameters are given in Table 1. X-ray diffraction data were collected at 130 K and room temperature on a Siemens Smart-CCD diffractometer using graphite-monochromated Mo Kα radiation ($\lambda = 0.710\ 73$ Å). For the low-temperature measurement, the crystal was "flash" cooled in a stream of cold nitrogen gas with no evident damage to the crystal. During data collection, the temperature was stable within ±1 °C even without the use of the feedback control of the low-temperature device.

**Table 1.** Crystallographic Data for $[Fe(ptz)_6](PF_6)_2$ at $T = 130(2)$ and 293(2) K

| | | |
|---|---|---|
| empirical formula: $C_{24}H_{48}F_{12}N_{24}P_2Fe$ | | fw 1018.65 |
| $Z = 1$ | | space group $P\bar{1}$ |
| $\lambda = 0.710\ 73$ Å | | |
| $T$, K | 130(2) | 293(2) |
| $a$, Å | 10.6439(4) | 10.8414(3) |
| $b$, Å | 10.8685(4) | 10.9776(4) |
| $c$, Å | 11.7014(4) | 12.0954(5) |
| α, deg | 75.644(1) | 74.936(1) |
| $\beta$, deg | 71.671(1) | 69.540(2) |
| $\gamma$, deg | 60.737(1 | 60.815(1) |
| $V$, Å$^3$ | 1114.52(7) | 1169.58(7) |
| $\rho_{calc}$, mg/m$^3$ | 1.518 | 1.446 |
| $\mu$, mm$^{-1}$ | 0.512 | 0.488 |
| final R1[a] ($I > 2\sigma$) | 0.0626 | 0.0615 |
| final wR2[b] (all data) | 0.1913 | 0.1627 |

[a] $R1 = \sum(|F_o| - |F_c|)/\sum|F_o|$. [b] $wR2 = [\sum w(F_o^2 - F_c^2)/\sum wF_o^2]^{1/2}$; $w = 1/[s^2(F_o^2) + (0.1192P)^2 + 2.3300P]$; $P = (F_o^2 + 2F_c^2)/3$.

A total of 1271 frames with a step width of 0.3° in $\omega$ and an exposure time of 10 s were collected at each temperature, corresponding to a hemisphere of intensity data. Cell constants were obtained by least-squares refinement on the $2\vartheta$ values of the sharpest 3949 reflections out of 4650 collected in the range $2.70 \leq 2\vartheta \leq 46.40°$ at low temperature and of 2777 reflections out of 4867 collected in the range $2.62 \leq 2\vartheta \leq 46.51°$ at room temperature. The collected frames were processed with the SAINT[42] program, which automatically performs Lorentz and polarization corrections; no absorption correction was applied.

The structure was solved by placing the iron atom at 0, 0, 0 (site symmetry $\bar{1}$) and locating all the other atoms by difference Fourier analysis. The refinement was done by full-matrix least-squares procedures on $F^2$ using SHELXL96[43] ($\beta$-test version). All non-hydrogen atoms were refined anisotropically, while hydrogen atoms, included at calculated positions, were refined in the riding mode with group temperature factors. Electron density corresponding to the counterions was modeled in terms of regular octahedra using rigid-body restraints: P−F distances were set to 1.579 Å ($w = 0.01$), F−F distances were set to $\sqrt{2}$(P−F), and differences in the components of the anisotropic displacements of all phosphorus and fluorine atoms were restrained to zero ($w = 0.001$) along the direction of interatomic vectors.

The propyl side chains and the counterion appear to be disordered at both temperatures, but the disorder could be described only for the counterion at room temperature by means of a model that takes into account three different orientations of the regular octahedron restraining the sum of occupation factors of the three different parts to be equal to 1.

**3. Optical Spectroscopy and Pressure Experiments.** Single-crystal absorption spectra in the region between 300 and 1300 nm were recorded on a Cary 5E spectrophotometer. For pressure experiments between 1 bar and 1 kbar, a single crystal of $[Fe(ptz)_6](PF_6)_2$ ($4 \times 3 \times 0.4$ mm$^3$) was mounted inside the helium-pressure cell described in ref 47. The cell was attached

(33) Franke, P. L.; Haasnot, J. G.; Zuur, A. P. *Inorg. Chim. Acta* **1982**, *59*, 5.
(34) Jung, J.; Bruchhäuser, F.; Feile, R.; Spiering, H.; Gütlich, P.; *Z. Phys. B* **1996**, *100*, 517.
(35) Jung, J.; Schmitt, G.; Wiehl, L.; Hauser, A.; Knorr, K.; Spiering, H.; Gütlich, P.; *Z. Phys. B* **1996**, *100*, 523.
(36) Decurtins, S.; Gütlich, P.; Köhler, C. P.; Hauser, A.; Spiering, H. *Inorg. Chem.* **1985**, *24*, 2174.
(37) Hauser, A. *J. Chem. Phys.* **1991**, *94*, 2741.
(38) Hauser, A. *Chem. Phys. Lett.* **1986**, *25*, 4245.
(39) Hauser, A. *Chem. Phys. Lett.* **1992**, *192*, 65.
(40) Wiehl, L. *Acta Crystallogr.* **1993**, *B49*, 289.
(41) Spiering, H.; Meissner, E.; Köppen, H.; Müller, E. W.; Gütlich P. *Chem. Phys.* **1982**, *68*, 65.
(42) *SAINT*, Version 4; Siemens Energy and Automation Inc.: Madison, WI, 1995.
(43) Sheldrick, G. M. SHELXL96: Program for the Refinement of Crystal Structures. University of Göttigen, Germany, 1996.

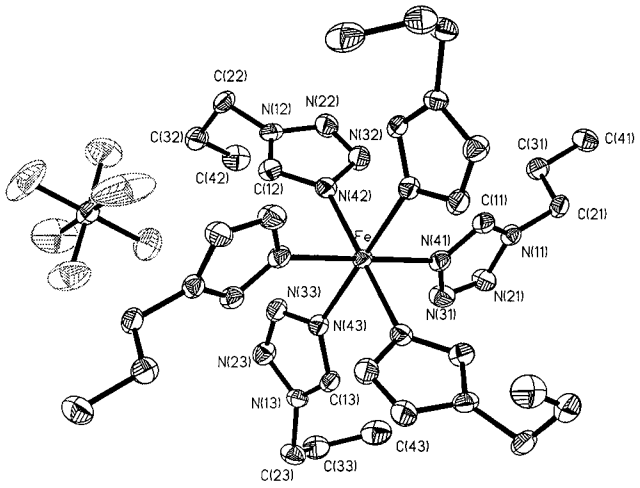


**Figure 1.** ORTEP[48] drawing of $[Fe(ptz)_6](PF_6)_2$ at 130 K with the appropriate atomic labelings. The displacement ellipsoids are given at the 50% probability level.

to the cold finger of a closed-cycle refrigerator (Air-Products, Displex CSA-202) equipped with optical windows. Temperature control was realized using a PID temperature controller (Scientific Instruments), with a Si diode (Lake Shore DT-470) in thermal contact with the cell. Hydrostatic He pressure of up to 1 kbar was achieved with a two-membrane pneumatic compressor (Novaswiss, Standard Type 554.3350).

In thermal equilibrium, the high-spin fraction as a function of temperature and pressure, $\gamma_{HS}$, was calculated from the area under the $^1A_1 \rightarrow {}^1T_1$ absorption band between 430 and 670 nm relative to the area at 20 K, for which $\gamma_{HS} = 0$.

The equilibrium curve at 1 bar was obtained by slowly cooling the sample within 8 h, which is necessary because of the very slow HS $\rightarrow$ LS relaxation at $T \leq 80$ K (vide infra), and then recording the spectra during slow warming. The curve at 10 bar was obtained by first applying an external pressure of ~500 bar in order to speed up the relaxation, then cooling the sample within 2 h, and subsequently releasing the pressure and collecting the spectra at 10 bar under slow warming. The curves under external pressure were obtained by two procedures: (A) cooling from room temperature with no pressure, applying the pressure at 20 K, and recording the spectra during warming; (B) applying the pressure at room temperature and recording the spectra during cooling.

Relaxation experiments following the quantitative population of the metastable high-spin state were performed by irradiating the whole crystal with 457 nm $Ar^+$ laser light, 40 mW, at $T =$ 15 K and a given pressure. The temperature was subsequently raised to the desired value between 50 and 74 K, and the HS $\rightarrow$ LS relaxation was monitored by recording absorption spectra in the region of the $^1A_1 \rightarrow {}^1T_1$ band at fixed time intervals. HS $\rightarrow$ LS relaxation curves $\gamma_{HS}(t)$ were extracted from the area under this band relative to the area for $t \rightarrow \infty$.

## Results and Discussion

**1. Crystal Structure.** Both at room temperature and at 130 K the title compound crystallizes in the triclinic space group $P\bar{1}$ with the iron atom placed on a center of inversion. In this report, only the low-temperature structure, which is similar to, but more accurate than, the room-temperature one, is discussed in detail. Furthermore 130 K is closer to the spin-transition temperature of 74(1) K at ambient pressure (vide infra).

An ORTEP[48] drawing of the title compound with the appropriate atomic labelings is shown in Figure 1, and some of the significant bond lengths and angles are collected in Table 2. The $FeN_6$ core shows almost regular octahedral coordination. The N−Fe−N bond angles are within 0.4° of 90.0°. The $[Fe(tetrazole)_6]^{2+}$ fragment shows approximate $\bar{3}$ symmetry with the relative pseudo axis perpendicular to the plane defined by N(41), N(42), and N(43) atoms.

**Table 2.** Selected Bond Lengths (Å) and Angles (deg) for $[Fe(ptz)_6](PF_6)_2$ at 130 K

| | | | |
|---|---|---|---|
| Fe−N(41) | 2.183(3) | C(21)−C(31) | 1.508(6) |
| Fe−N(42) | 2.199(3) | C(31)−C(41) | 1.530(6) |
| Fe−N(43) | 2.181(3) | P−F(6) | 1.553(4) |
| N(41)−C(11) | 1.314(6) | P−F(4) | 1.580(3) |
| N(41)−N(31) | 1.372(5) | P−F(5) | 1.583(3) |
| N(31)−N(21) | 1.306(5) | P−F(2) | 1.584(3) |
| N(21)−N(11) | 1.354(5) | P−F(3) | 1.584(3) |
| N(11)−C(11) | 1.331(6) | P−F(1) | 1.594(3) |
| N(11)−C(21) | 1.474(5) | | |
| N(41)−Fe−N(41) | 179.999(1) | N(43)−Fe−N(42) | 90.62(13) |
| N(41)−Fe−N(42) | 88.82(13) | N(43)−Fe−N(41) | 90.19(13) |

Two of the three crystallographically inequivalent ligands show similarities both in the *gauche* conformation of the side chains and in the displacement of the tetrazole plane with respect to the N(41)−N(42)−N(43) plane (−46°, −48°). The third ligand adopts a trans conformation of the side chain, and the dihedral angle between the two planes is approximately 58°. Also, the Fe−N(41) distance is slightly but significantly longer (2.199(3) Å) than the other two (2.181(3), 2.183(3) Å). These values are typical for the HS state.

All the bond lengths in the side chains are slightly shorter than the expected values, due to disorder between the other possible conformations. In the refinement, no model to describe the disorder has been taken into account, and this also leads to large values of the anisotropic displacement parameters for the corresponding atoms. The structure is ordered in layers orthogonal to the pseudo-3-fold axis of rotation. Such a pseudotrigonal symmetry of the complex layers seems to be a general structural feature within the $[Fe(Rtz)_6](X)_2$ series (R = methyl, ethyl, propyl; X = $BF_4^-$, $PF_6^-$).[40,44−46] Figure 2 shows a packing diagram of one of these layers, with the projection taken along the normal to the plane defined by the three independent nitrogens attached to the central iron atom. This direction is very close to that of the $c^*$ axis.

Direct comparison of the structure of the title compound with that of the analogous $[Fe(ptz)_6](BF_4)_2$ compound[40] shows a practically indistinguishable bidimensional arrangement of the layers. Interplanar spacings are very similar in the two structures (11 Å for $[Fe(ptz)_6](BF_4)_2$ and 10.8 Å for $[Fe(ptz)_6](PF_6)_2$), but the relative packing of consecutive planes is completely different. Weak interactions of the propyl side chains determine interlayer contacts in the title compound (Figure 3); thus the interlayer plane is the principal cleavage direction in the crystal.

**2. Spin Equilibrium and Photophysical Properties.** The highly temperature-dependent single-crystal absorption spectra shown in Figure 4 at ambient pressure prove the compound $[Fe(ptz)_6](PF_6)_2$ to be a spin-crossover system. At room temperature, there is one absorption band in the near-IR corresponding to the only spin-allowed d−d transition of the HS species, $^5T_2 \rightarrow {}^5E$. At 74 K, only a fraction of the complexes remain in the HS state and the intensity of the $^5T_2 \rightarrow {}^5E$ band

(44) Hinek, R.; Gütlich, P.; Hauser, A. *Inorg. Chem.* **1994**, *33*, 567.
(45) Hinek, R.; Spiering, H.; Schollmeyer; Gütlich, P.; Hauser, A. *Chem. Eur. J.* **1996**, *1*, 1427.
(46) Hinek, R.; Spiering, H.; Gütlich, P.; Hauser, A. *Chem. Eur. J.* **1996**, *1*, 1435.
(47) Jeftić, J.; Kindler, U.; Spiering, H.; Hauser, A. *Meas. Sci. Technol.* **1997**, *5*, 479.
(48) Johnson, C. K. *ORTEP II*; Report ORNL-5138; Oak Ridge National Laboratory: Oak Ridge, TN, 1976.

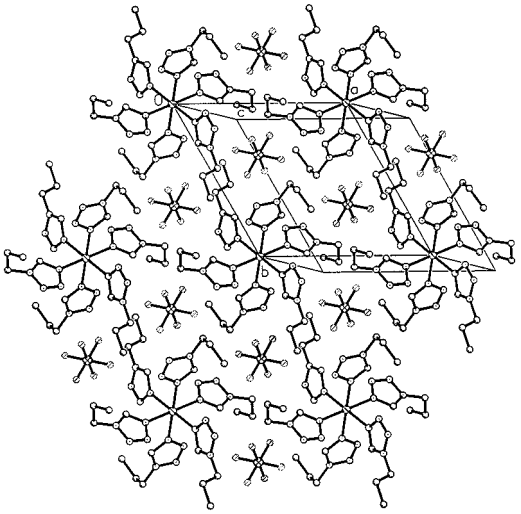

**Figure 2.** Packing diagram of layers in projection along the pseudo-trigonal axis normal to the N(41)−N(42)−N(43) plane of $[Fe(ptz)_6](PF_6)_2$.

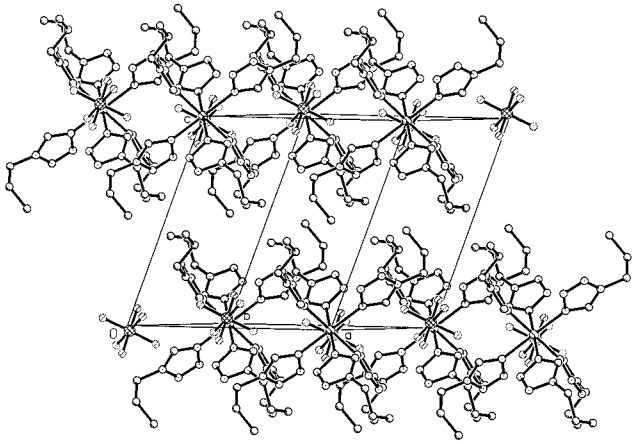

**Figure 3.** Three-dimensional packing diagram of $[Fe(ptz)_6](PF_6)_2$ showing the interlayer contacts.

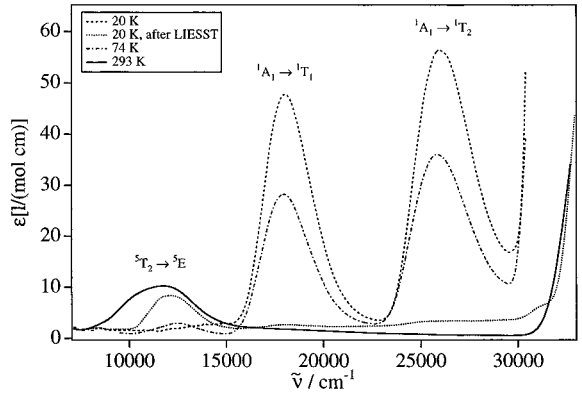


**Figure 4.** Single-crystal absorption spectra of $[Fe(ptz)_6](PF_6)_2$ at 293, 74, and 20 K before and after irradiation at 457 nm.

decreases, while two new spin-allowed d−d bands due to the $^1A_1 \rightarrow {}^1T_1$ and $^1A_1 \rightarrow {}^1T_2$ transitions confirm a population of the LS state. Below 50 K, the system is completely in its ground state, and only the $^1A_1 \rightarrow {}^1T_1$ and $^1A_1 \rightarrow {}^1T_2$ bands are present. At such low temperatures, using the effect of **l**ight **i**nduced **e**xcited **s**pin **s**tate **t**rapping (LIESST),[36,37] it is possible to populate the HS state quantitatively as a metastable state by irradiating into one of the LS bands. The absorption spectrum at 20 K following irradiation with the 457 nm line of the $Ar^+$ laser is included in Figure 4 (irradiation at the edge of the $^1A_1 \rightarrow {}^1T_1$ band helps to preserve crystal quality). It again shows the typical HS band in the near-IR. At ambient pressure and temperatures below 30 K, the complexes remain in the light-induced HS state for several days.

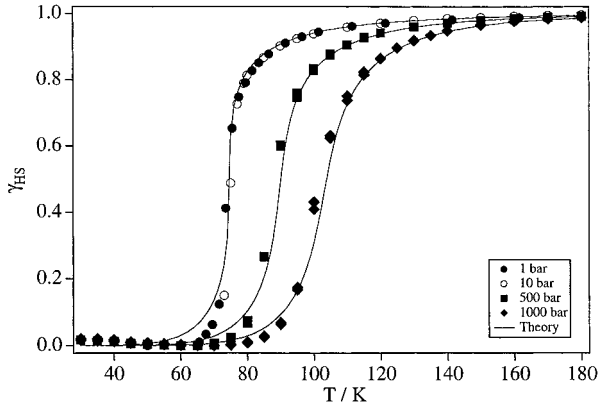


**Figure 5.** Experimental and calculated transition curves of $[Fe(ptz)_6](PF_6)_2$ at 1, 10, 500, and 1000 bar.

Figure 5 shows the experimental transition curves, that is the HS fraction, $\gamma_{HS}$, as a function of temperature, obtained from temperature-dependent optical spectra as described in the Experimental Section, at pressures of 1, 10, 500, and 1000 bar. At 1 bar, the thermal spin transition is quite abrupt with a transition temperature $T_{1/2}$ (the temperature for which $\gamma_{HS} = 0.5$) of 74(1) K. An external pressure stabilizes the LS state because of its smaller volume, resulting in a shift of $T_{1/2}$ to higher temperatures upon increasing pressure. The experimental shift $\Delta T_{1/2}$ is found to be = 28(1) K/kbar. In contrast to the case of $[Fe(ptz)_6](BF_4)_2$,[36] there is no hysteresis at ambient pressure in $[Fe(ptz)_6](PF_6)_2$, nor is there one induced by an external pressure as in $[Zn_{1-x}Fe_x(ptz)_6](BF_4)_2$, x = 0.1,[28] indicating the absence of any crystallographic phase transition in the $PF_6^-$ derivative.

The above is substantiated by Mössbauer spectra and magnetic susceptibility measurements.[49] The transition curves obtained at 1 bar using the two methods are in good agreement with the one obtained from optical spectroscopy. The Mössbauer spectrum at 130 K consists of a single quadrupole doublet ($\delta$ = 1.03 mm/s, $\Delta E_Q$ = 1.45 mm/s) typical for high-spin iron(II), whereas at 30 K the signal consists of a single line ($\delta$ = 0.45 mm/s, $\Delta E_Q$ < 0.1 mm/s) typical for low-spin iron(II) in a close to octahedral environment. The line widths of 0.24 and 0.3 mm/s, respectively, and the quadrupole splittings show no anomalies in the temperature interval of the spin transition, supporting the statement that in the $PF_6^-$ salt there is no crystallographic phase transition.

**3. Determination of the Thermodynamic Parameters.** The Gibbs free energy of a neat spin-crossover system containing a random distribution of $\gamma_{HS}$ complexes in the HS state and $\gamma_{LS} = 1 - \gamma_{HS}$ complexes in the LS state can be written as[3,41,50]

$$G(\gamma_{HS}, p, T) = \gamma_{HS}\,[\Delta F^{\circ}_{HL}(T) + p\Delta V^{\circ}_{HL}] - TS_{mix}(\gamma_{HS}) + G^{int}(\gamma_{HS}) \quad (1)$$

All $\gamma_{HS}$-independent terms have been omitted. $\Delta F^{\circ}_{HL}(T) = F^{\circ}_{HS}(T) - F^{\circ}_{LS}(T)$ corresponds to the free energy difference between the HS and the LS state in a given reference lattice in the absence of interactions and at 1 bar. It can, for instance, be directly determined from transition curves obtained for highly diluted mixed crystals, with the iron(II) complex doped into an

(49) Hinek, R. Diploma Thesis, University of Mainz, Germany, 1990.
(50) Köhler, C. P.; Jakobi, R.; Meissner, E.; Wiehl, L.; Spiering, H.; Gütlich, P. *J. Phys. Chem. Solids* **1990**, *51*, 239.

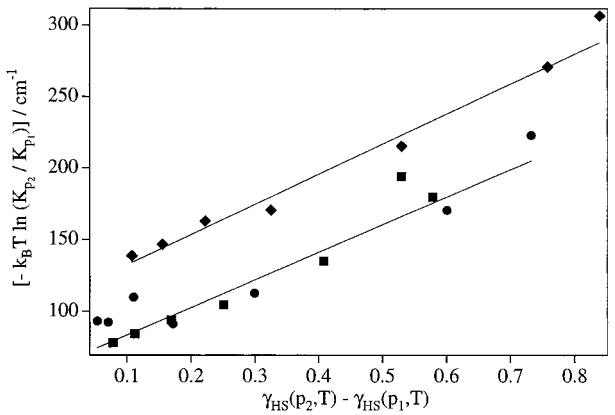


**Figure 6.** Plot of $[-k_BT \ln(K_{p_2}/K_{p_1})]$ vs $[\gamma_{HS}(p_2, T) - \gamma_{HS}(p_1, T)]$ for $p_2 = 500$ bar and $p_1 = 10$ bar (●), $p_2 = 1000$ bar and $p_1 = 500$ bar (■), and $p_2 = 1000$ bar and $p_1 = 10$ bar (◆). Linear regression fit to the data (—) with $\Delta p = 500$ bar (●, ■) and 1000 bar (◆): slopes $2\Gamma =$ 194(9) and 210(8) $cm^{-1}$ and intercepts $(\Delta p)\Delta V^\circ_{HL} = 62(4)$ and 112(4) $cm^{-1}$, respectively.

isomorphous host lattice.[41,51] $\Delta V^\circ_{HL} = V^\circ_{HS} - V^\circ_{LS}$ is the difference in volume between the two states, $S_{mix} = -k_B[\gamma_{HS} \ln \gamma_{HS} + (1 - \gamma_{HS}) \ln(1 - \gamma_{HS})]$ is the mixing entropy for the neat compound, and $G^{int}$ accounts for all interactions between the spin-changing molecules. In mean-field approximation, the latter can be expanded in the following form:[3,41,50]

$$G^{int}(\gamma_{HS}) = \Delta\gamma_{HS} - \Gamma\gamma_{HS}^2 \tag{2}$$

The interaction constant $\Gamma$ describes the interaction between HS and LS complexes; the lattice shift $\Delta$ depends upon their interaction with the reference lattice. In the following, the temperature dependence of $\Delta$ and $\Gamma$ is assumed to be negligible.[52]

In thermal equilibrium, the condition

$$\left(\frac{\partial G}{\partial \gamma_{HS}}\right)_{T,p} = 0 \tag{3}$$

results in the implicit equation of state

$$\Delta F^\circ_{HL}(T) + p\Delta V^\circ_{HL} + \Delta - 2\Gamma\gamma_{HS} + k_BT \ln\left[\frac{\gamma_{HS}}{1 - \gamma_{HS}}\right] = 0 \tag{4}$$

By performing measurements at different pressures, one can determine both $\Delta V^\circ_{HL}$ and $\Gamma$ without any prior knowledge of $\Delta F^\circ_{HL}(T)$ and $\Delta$. From eq 4 it follows that, at a given temperature and two different pressures, the relation

$$(p_2 - p_1)\Delta V^\circ_{HL} - 2\Gamma[\gamma_{HS}(p_2, T) - \gamma_{HS}(p_1, T)] = -k_BT \ln\left[\frac{[\gamma_{HS}(p_2, T)][1 - \gamma_{HS}(p_1, T)]}{[1 - \gamma_{HS}(p_2, T)][\gamma_{HS}(p_1, T)]}\right] \tag{5}$$

holds.[31] Figure 6 shows a plot of the right hand side of eq 5 vs $[\gamma(p_2, T) - \gamma(p_1, T)]$ obtained from the transition curves for $p_2 = 500$ bar and $p_1 = 1$ bar, $p_2 = 1000$ bar and $p_1 = 500$ bar, and $p_2 = 1000$ bar and $p_1 = 1$ bar. A linear fit to the experimental points gives a mean value of the slope of 202(10) $cm^{-1}$, corresponding to a value for $\Gamma$ of 101(5) $cm^{-1}$, and

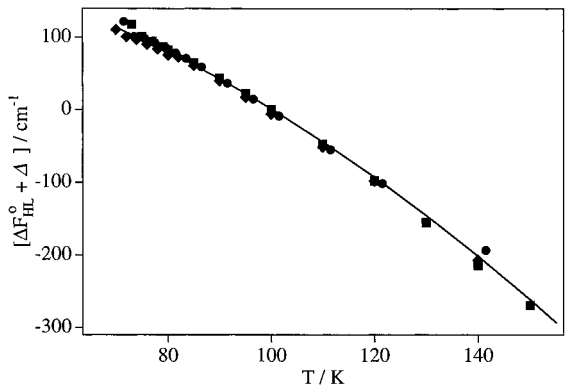


**Figure 7.** $[\Delta F^\circ_{HL}(T) + \Delta]$ from three independent measurements of the transition curve at 1 bar (●, ■, ◆), together with the second-order polynomial fit (—).

intercepts of 62(4) and 112(4) $cm^{-1}$ for $p_2 - p_1 = 500$ and 1000 bar, respectively, yielding a value for $\Delta V^\circ_{HL}$ of 24(3) $Å^3$/molecule.

Using the above values of $\Delta V^\circ_{HL}$ and $\Gamma$, it is now possible to extract $\Delta F^\circ_{HL}(T) + \Delta$ from the experimental transition curves using eq 4. Only their sum is uniquely defined, but their individual values depend upon the choice of reference lattice. Figure 7 shows $\Delta F^\circ_{HL}(T) + \Delta$ for three independent measurements of the transition curve at 1 bar. $\Delta F^\circ_{HL}(T) + \Delta$ does not depend linearly on temperature. Indeed, it is not expected to do so, because at low temperatures $\Delta H^\circ_{HL}(T)$ and $\Delta S^\circ_{HL}(T)$ both are known to show comparatively strong dependence on temperature.[2,34,35,51] Within the temperature interval of the experimental points of Figure 7, $\Delta F^\circ_{HL}(T) + \Delta$ is well described empirically by a polynomial of second order, giving values of $\Delta H^\circ_{HL}(T_{1/2}) + \Delta$ and $\Delta S^\circ_{HL}(T_{1/2})$ of 357(3) $cm^{-1}$ and 3.45(4) $cm^{-1}$/K, respectively. In Figure 5 the transition curves calculated using the above polynomial fit and setting $\Gamma = 101$ $cm^{-1}$ and $\Delta V^\circ_{HL} = 24$ $Å^3$ for $p = 1$, 500, and 1000 bar are shown. The overall agreement between experimental and calculated curves is satisfactory.

Equation 4, the implicit equation of state, has been discussed in detail by Köhler et al.[50] and has been shown to be equivalent to the van der Waals equation of state. The so-called reduced pressure[50]

$$\Pi^* = \frac{\Delta F^\circ_{HL}(T) + \Delta + p\Delta V^\circ_{HL}}{\Gamma} \tag{6}$$

relates the total energy separation between the HS and LS states, $\Delta F^\circ_{HL}(T) + \Delta + p\Delta V^\circ_{HL}$, to the interaction energy $\Gamma$. If $\Pi^*$ evaluated at the critical temperature (in the sense of a van der Waals gas)

$$T_c = \frac{\Gamma}{2k_B} \tag{7}$$

is less than 1, the spin transition is expected to occur as a first-order phase transition with a hysteresis. For $\Pi^*$ larger than 1, the spin transition is continuous and fully reversible. With $\Gamma = 101$ $cm^{-1}$, $T_c$ becomes equal to 73 K and $\Pi^*$ equal to 1.03 at 1 bar, 1.62 at 500 bar, and 2.22 at 1000 bar. Thus for $p =$ 1 bar, the system is very close to the critical isobar, and consequently the transition curve is extremely steep, with $T_{1/2}$ almost equal to $T_c$. External pressure shifts the system away from the critical isobar, transition curves move to higher temperatures and become more gradual.

**4. Kinetics of the HS → LS Relaxation.** The temperature dependence of the HS → LS relaxation is shown in Figure 8.

(51) Jakobi, R.; Spiering, H.; Wiehl, L.; Gmelin, E.; Gütlich, P. *Inorg. Chem.* **1988**, *27*, 1823.
(52) Adler, P.; Wiehl, L.; Meissner, E.; Köhler, C. P.; Spiering, H.; Gütlich, P. *J. Phys. Chem. Solids* **1987**, *48*, 517.

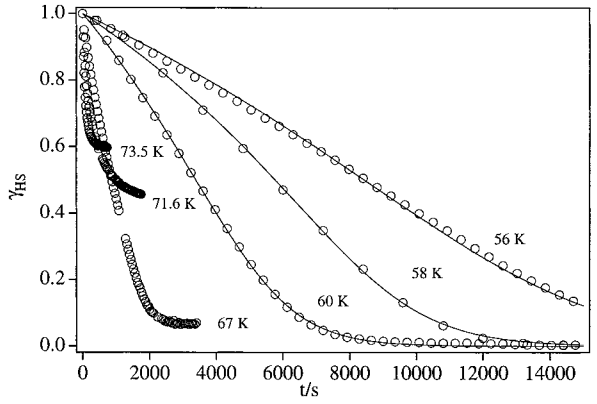


**Figure 8.** HS → LS relaxation curves for $[Fe(ptz)_6](PF_6)_2$ following irradiation at 457 nm at ambient pressure and temperatures between 50 and 74 K.

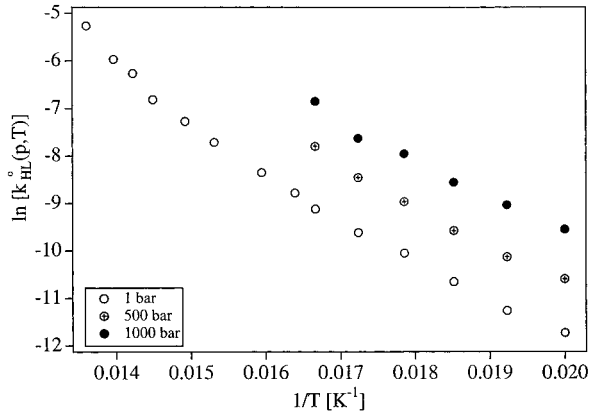


**Figure 9.** Arrhenius plot of the initial rate constant $k^{\circ}_{HL}(p, T)$ for the HS → LS relaxation of $[Fe(ptz)_6](PF_6)_2$ plotted as $\ln[k^{\circ}_{HL}(p, T)]$ vs $1/T$ at pressures of 1, 500, and 1000 bar.

At higher temperatures the relaxation proceeds faster, but above 65 K it is no longer complete, $\gamma_{HS}(t \rightarrow \infty)$ shifting toward the value given by the transition curve in Figure 5. The relaxation curves show a sigmoidal behavior, which is an indication of cooperative effects and can be quantitatively described with a relaxation rate constant depending upon the LS fraction according to

$$k_{HL}(\gamma_{LS}, T) = k_{HL}(\gamma_{LS} = 0, T)\exp(\alpha\gamma_{LS}) = k^{\circ}_{HL}(T)\exp(\alpha\gamma_{LS}) \quad (8)$$

Numerical fits to the experimental curves give a value for the self-acceleration factor $\alpha$ of 2.1(2) corresponding to an increase of 1 order of magnitude from the initial to the final relaxation rate constant. Between 50 and 60 K, that is for temperatures below $T_{1/2}$, $\alpha$ is within experimental error independent of temperature.

Fast cooling of the compound (from 90 to 20 K within 30 s) results in an almost quantitative thermal quenching of the compound in the metastable HS state. Relaxation curves in the temperature region 65−68 K identical with the ones obtained after irradiation at 20 K are observed.[49] This is a further indication that just one crystallographic phase is present.

Figure 9 depicts the initial rate constant $k^{\circ}_{HL}(T)$ at 1 bar for temperatures between 50 and 74 K plotted as $\ln[k^{\circ}_{HL}(T)]$ vs $1/T$ (Arrhenius plot). Even within this comparatively small temperature interval, the deviation from classical linear behavior is obvious. This is not surprising because this temperature interval is between the low-temperature tunneling region with its only slightly temperature-dependent tunneling rate constant and the high-temperature region with a thermally activated process.[53]

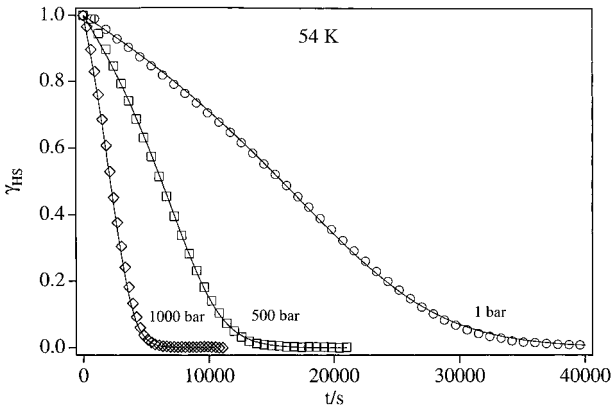


**Figure 10.** HS → LS relaxation curves for $[Fe(ptz)_6](PF_6)_2$ at 54 K at pressures of 1, 500, and 1000 bar.

Figure 10 shows the HS → LS relaxation curves at $T = 54$ K and pressures of 1, 500, and 1000 bar. The sigmoidal curves are still well described by eq 8, but now the initial rate constant is also a function of pressure, $k^{\circ}_{HL}(p, T)$. A numerical fit to the experimental curves of Figure 10 results in a value for $\alpha$ of 2.0(2), which is in the above range and within experimental error independent of pressure.

The initial rate constant $k^{\circ}_{HL}(p, T)$ at external pressures is included in Figure 9. The external hydrostatic pressure acts isotropically on the whole crystal and accelerates the HS → LS relaxation exponentially as follows:

$$k_{HL}(\gamma_{LS}, p, T) = k^{\circ}_{HL}(p, T)\exp(\alpha\gamma_{LS}) = k^{\circ}_{HL}(T)\exp(\alpha\gamma_{LS} + \beta p) \quad (9)$$

Within the temperature interval 50−60 K, the acceleration factor $\beta$ is almost constant, with values ranging from 2.2(1) $kbar^{-1}$ at 50 K to 2.0(1) $kbar^{-1}$ at 60 K. This corresponds to an increase in HS → LS relaxation rate constant by 1 order of magnitude per kilobar. An external pressure of 1 kbar thus accelerates the HS → LS relaxation by the same amount as the cooperative effects. In the physically most simple interpretation of the latter as a changing internal pressure, the change in such an internal pressure during the relaxation is therefore equal to 1 kbar, which is on the order of $\Gamma/\Delta V^{\circ}_{HL}$.

**5. Energy Shift of the $^1A_1 \rightarrow {}^1T_1$ Band as a Function of Temperature, Pressure, and the Low-Spin Fraction.** Figure 11 shows the shift of the maximum of the $^1A_1 \rightarrow {}^1T_1$ band, $\tilde{\nu}_{max}$, with pressure at 50 and 73 K. At 50 K, which is well below the transition temperature, and $\gamma_{LS} = 1$, $\tilde{\nu}_{max}$ increases linearly with external pressure:

$$\tilde{\nu}_{max} = \tilde{\nu}_{max}(p \rightarrow 0) + \Delta\tilde{\nu}_p p \quad (10)$$

From the slope of the curve in Figure 11 values for $\tilde{\nu}_{max}(p \rightarrow 0)$ and $\Delta\tilde{\nu}_p(^1T_1)$ of 18125(2) and 36(3) $cm^{-1}$/kbar, respectively, result. In this very close to octahedral complex, the shift is mainly due to an increase of the ligand-field strength $10Dq^{LS}$ as a result of the compression of the M−L bond length in the LS state, $r_{LS}$, by the external pressure according to

$$\frac{r_{LS}(p)}{r_{LS}(p \rightarrow 0)} = \left(\frac{10Dq^{LS}(p \rightarrow 0)}{10Dq^{LS}(p)}\right)^{1/n} \quad (11)$$

(53) Hauser, A. *Comments Inorg. Chem.* **1995**, *17*, 17.

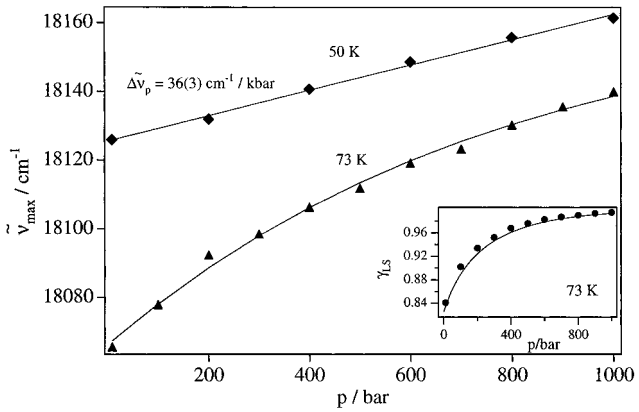


**Figure 11.** Shift of the $^1A_1 \rightarrow {}^1T_1$ band maximum of $[Fe(ptz)_6](PF_6)_2$ as a function of pressure at 50 and 73 K. Inset: $\gamma_{LS}$ as a function of external pressure.

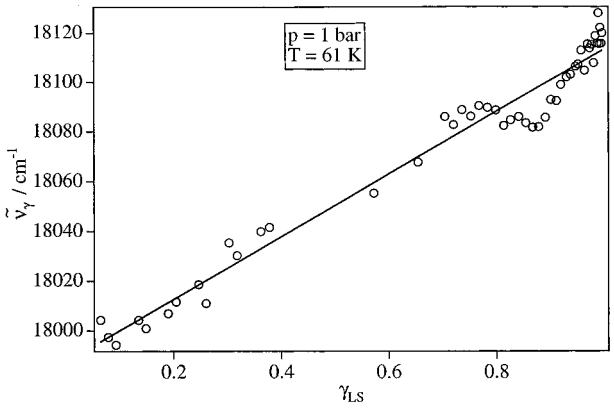


**Figure 12.** Shift of the $^1A_1 \rightarrow {}^1T_1$ band maximum of $[Fe(ptz)_6](PF_6)_2$ as a function of $\gamma_{LS}$ during the HS $\rightarrow$ LS relaxation at 61 K and 1 bar.

where $n = 5-6$.[54] The change of the LF strength with pressure can be written as $\delta 10Dq^{LS}(p)$, and the change in the Fe−N distance, as $\delta r_{LS}(p)$. The much smaller value of $\delta 10Dq^{LS}(p)$ as compared to the absolute value of the LF strength itself allows the approximation

$$\frac{\delta r_{LS}(p)}{r_{LS}(p \rightarrow 0)} = -\frac{1}{6}\left(\frac{\delta\ 10Dq^{LS}(p)}{10Dq^{LS}(p \rightarrow 0)}\right) = -\frac{\Delta\tilde{\nu}_p p}{6(10Dq^{LS}(p \rightarrow 0))} \quad (12)$$

with $\delta\ 10Dq^{LS}(p) \approx \Delta\tilde{\nu}_p p$, because in the Tanabe−Sugano diagram the $^1T_1$ energy depends linearly on $10Dq$ with slope 1.[54] With the above value for $\Delta\tilde{\nu}_p$ and the value for $10Dq^{LS}(p \rightarrow 0)$ of 20 200 cm$^{-1}$,[37] the estimated change in metal−ligand bond length $\delta r_{LS}(p)$ caused by the external pressure is $\approx -6 \times 10^{-4}$ Å/kbar. In the context of the relaxation dynamics, however, the relevant quantity is the change in bond length difference $\delta\Delta r_{HL}(p)$. Since the force constants of the LS state are typically not more than 50% higher than those of the LS state,[35] $\delta r_{HS}(p)$ is only expected to be slightly larger than $\delta r_{LS}(p)$. In the low-pressure regime, $\delta\Delta r_{HL}(p)$ is thus negligible, and in a first approximation, this allows the crude assumption that $\Delta V^\circ_{HL}(p) = \Delta V^\circ_{HL}(p \rightarrow 0)$.

At 73 K, that is, at a temperature near $T_{1/2}$, and ambient pressure, a fraction of the complexes is in the HS state, as shown in the inset of Figure 11. With application of an external pressure, the spin equilibrium shifts from the initial value of $\gamma_{LS} = 0.84$ at 10 bar to $\gamma_{LS} = 0.995$ at 1000 bar. The corresponding shift of $\tilde{\nu}_{max}$ is included in Figure 11. The curve is no longer linear and shows that $\tilde{\nu}_{max}$ is a function of $\gamma_{LS}$, $T$, and $p$ simultaneously. It shifts toward lower values for increasing temperature, as is evident from a direct comparison at a pressure of 1000 bar for which $\gamma_{LS} \rightarrow 1$ for both curves. It is, however, not straightforward to disentangle the pressure dependence and the dependence on $\gamma_{LS}$ of $\tilde{\nu}_{max}$ quantitatively from the curve in Figure 11. Qualitatively, and as expected, an increasing LS fraction corresponds to an increasing internal pressure.

Alternatively the $\gamma_{LS}$ dependence of $\tilde{\nu}_{max}$ can be determined during the HS $\rightarrow$ LS relaxation at constant temperature and constant pressure. In Figure 12, $\tilde{\nu}_{max}$ as a function of $\gamma_{LS}$ during the relaxation at a temperature of 61 K and ambient pressure is shown. $\tilde{\nu}_{max}$ is linear in $\gamma_{LS}$ with a slope $\Delta\tilde{\nu}_\gamma$ of 125(6) cm$^{-1}$ and $\tilde{\nu}_{max}$ at $\gamma_{LS} = 1$ equal to 18114(5) cm$^{-1}$.

From the comparison of the self-acceleration factor of the HS $\rightarrow$ LS relaxation $\alpha$ with the acceleration factor from the external pressure $\beta$, it was concluded that the internal pressure change is on the order of 1 kbar. But, surprisingly, $\Delta\tilde{\nu}_\gamma$ is more than 3 times larger than $\Delta\tilde{\nu}_p$. This can be explained on the basis of the crystal packing. The layer structure results in a comparatively strong anisotropy of the compressibility. Thus, not only could an external pressure induce bond length changes, as assumed above, but it could, for instance, also compress the complexes along the pseudotrigonal axis. In addition to a shift, the $^1T_1$ state would also split, leading to a broadening of the band under external pressure. Such a broadening is indeed observed experimentally. The elastic interactions primarily influence the bond length changes in much the same way as the external pressure. But their influence on other than the totally symmetric Fe−N stretching vibrations is certainly different, leading to different shifts and splittings than the external pressure. A direct, quantitative comparison of $\Delta\tilde{\nu}_\gamma$ and $\Delta\tilde{\nu}_p$ is therefore difficult.

## Conclusions

We have presented a comprehensive treatment of the thermal spin transition and the HS $\rightarrow$ LS relaxation in $[Fe(ptz)_6](PF_6)_2$. Even within the comparatively crude model of the elastic interactions, that is, regarding them as a changing internal pressure, a consistent picture of the thermal equilibrium and the relaxation kinetics emerged.

The related system $[Fe(ptz)_6](BF_4)_2$ has an interaction constant $\Gamma$ of 170 cm$^{-1}$ in the high-symmetry phase[28] and of 138 cm$^{-1}$ in the low-symmetry phase,[55] with corresponding values for $\Delta V^\circ_{HL}$ of 26[28] and 35 Å$^3$/molecule,[20] respectively. The values for the title compound are 101 cm$^{-1}$ and 24 Å$^3$/molecule for $\Gamma$ and $\Delta V^\circ_{HL}$, respectively. There is no direct correlation between $\Gamma$ and $\Delta V^\circ_{HL}$. In order to treat the interaction constant $\Gamma$ quantitatively, the elastic properties of the material would have to be known explicitly, and the various contributions, that is, image pressure contribution and isotropic and anisotropic direct contributions, would have to be evaluated individually.[34,35,56,57] Whereas all pressure type (isotropic) interactions basically do scale with $\Delta V^\circ_{HL}$ and give positive contributions to $\Gamma$,[41] anisotropic interactions may also give negative contributions,[34,35] which depend very much upon the actual crystal packing.

(54) Schläfer, H. L.; Gliemann, G. Einführung in die Ligandenfeldtheorie; Akademische Verlagsgesellschaft: Wiesbaden, Germany, 1980, p 462.
(55) Jeftić, J.; Hauser, A. Manuscript in preparation.
(56) Willenbacher, N.; Spiering, H. *J. Phys. C: Solid State Phys.* **1988**, *21*, 1423.
(57) Spiering, H.; Willenbacher, N. *J. Phys. Condens. Matter* **1989**, *1*, 10089.

Although, in principle, the interaction constant depends on pressure, as pressure reduces the crystal volume and the strength of intermolecular contacts increases, the comparatively low pressures applied in this study are not large enough to be effective in this respect. The relaxation experiments, in fact, yield a pressure-independent interaction constant.

The title compound proved to be ideal for the present study, because $\Gamma$ is large but just below the critical value above which the additional complication of a hysteresis in the thermal spin transition would have to be accounted for and because there is no crystallographic phase transition. The title compound would also be ideal for a crystallographic low-temperature study with a single-crystal structure determination above and below $T_{1/2}$ as well as following irradiation at low temperatures.

**Acknowledgment.** We thank Harald Romstedt for helpful discussions, Ueli Kindler for building the pressure cell, and Hans U. Güdel, Philipp Gütlich, and Hans-Beat Bürgi for the use of equipment. This work was financially supported by the Schweizerischer Nationalfonds and the Deutsche Forschungsgemeinschaft.

**Supporting Information Available:** Tables of crystal data and structure refinement details, atomic coordinates and equivalent isotropic displacement parameters for non-hydrogen atoms, full bond lengths, angles, and torsion angles, anisotropic displacement parameters for non-hydrogen atoms, and coordinates and isotropic displacement parameters for hydrogen atoms (17 pages). Ordering information is given on any current masthead page.

IC961404O